Journal of Pharmaceutical and Biomedical Analysis 48 (2008) 1310–1315

Contents lists available at ScienceDirect

Journal of Pharmaceutical and Biomedical Analysis

journal homepage: www.elsevier.com/locate/jpba

Raman detected differential scanning calorimetry of polymorphic transformations in acetaminophen

John F. Kauffman[a,*], Linda M. Batykefer[b], David D. Tuschel[b]

[a] Food and Drug Administration, Center for Drug Evaluation and Research, Division of Pharmaceutical Analysis, 1114 Market Street, St. Louis, MO 63101, United States
[b] ChemImage Corporation, 7301 Penn Avenue, Pittsburgh, PA, United States

ARTICLE INFO

Article history:
Received 1 July 2008
Received in revised form 28 August 2008
Accepted 4 September 2008
Available online 11 September 2008

Keywords:
Raman spectroscopy
Differential scanning calorimetry
Polymorphism
Acetaminophen

ABSTRACT

Acetaminophen is known to crystallize in three polymorphic forms. Thermally induced transformations between the crystalline forms and the super-cooled liquid have been observed by differential scanning calorimetry (DSC), but the assignment of calorimetric transitions to specific polymorphic transformations remains challenging, because the transition temperatures for several transformations are close to one another, and the characteristics of the observed transitions depend on experimental variables that are often poorly controlled. This paper demonstrates the simultaneous application of DSC and Raman microscopy for the observation of thermally driven transitions between polymorphs of pharmaceutical materials. Raman detected differential scanning calorimetry (RD-DSC) has been used to monitor the DSC thermograms of super-cooled liquid acetaminophen and confirms the assignment of two exothermic transitions to specific polymorphic transformations. Principal component analysis of the Raman spectra have been used to determine the number of independent components that participate in the phase transformations, and multivariate regression has been used to determine transition temperatures from the spectral data. The influence of the laser excitation source on measured DSC thermograms has also been investigated, and it has been demonstrated that a baseline shift occurs in RD-DSC when a polymorphic transformation occurs between crystalline and amorphous forms. RD-DSC has been used to examine the influence of sample aging and sample pan configuration on the observed polymorphic transformations, and both of these variables were found to influence the thermal behavior of the sample. The results demonstrate the advantage of simultaneous Raman spectroscopy and differential scanning calorimetry for the unambiguous assignment of thermally driven polymorphic transformations.

Published by Elsevier B.V.

1. Introduction

Acetaminophen (*N*-acetyl *para*-amino phenol, APAP) is known to have three crystalline polymorphs [1,2]. Monoclinic type I APAP is the thermodynamically stable polymorph that is found in commercial products. Orthorhombic type II APAP is a metastable polymorph that is stable on a timescale of months in powder form at room temperature [3]. Types I and II APAP can be distinguished from one another by their melting temperatures, X-ray structures and spectroscopic characteristics. Type III APAP is highly unstable, and its single crystal X-ray structure has not been determined to date, but it has been observed spectroscopically in thin film samples, and powder X-ray diffraction patterns have been published [4]. Several authors have noted that type I APAP has poor compression properties [1,5,6], and considerable effort has been devoted to producing directly compressible pure APAP powders. Fachaux et al. [6,7] have utilized particle engineering techniques to prepare sintered, crystalline type I APAP that was found to have good compression properties. Other groups have pursued strategies for the production of type II APAP, which is known to be directly compressible [8]. Di Martino et al. [3] prepared type II APAP by recrystallization of the amorphous super-cooled liquid (SCL) formed by cooling molten APAP. Nichols and Frampton [1] crystallized type II APAP from denatured ethanol by seeding a cold, supersaturated solution with type II crystals. Their seed crystals were prepared by recrystallization of the SCL. Lang et al. [9] demonstrated that several commercially available polymers can be used as templates to direct the formation of type II APAP.

Preparation of type II APAP from the SCL has been demonstrated by several authors in differential scanning calorimetry (DSC) thermograms on the milligram scale [2,10–13]. Qi et al. have recently summarized the literature on this topic [13]. Type I APAP melts at approximately 169 °C, with reported melting transitions occurring over the 157–172 °C range. If the molten liquid is held at high tem-

* Corresponding author. Tel.: +1 314 539 2168.
E-mail address: John.Kauffman@fda.hhs.gov (J.F. Kauffman).

0731-7085/$ – see front matter. Published by Elsevier B.V.
doi:10.1016/j.jpba.2008.09.008

perature long enough to ensure the elimination of all crystals, the material remains amorphous upon cooling to room temperature. If the sample is immediately reheated, the DSC thermogram exhibits a relatively large exothermic transition in the 60–80 °C range, and under some circumstances a second exotherm is observed in the 100–120 °C range. These exothermic transitions are followed by a melting transition, which can be assigned to melting of type III (156 °C), type II (158 °C) or type I (171 °C) based on the onset temperature. When both exotherms are observed, they are usually followed by a type II melting transition. Qi et al. [13] have demonstrated that the characteristics of the observed exothermic transitions depend on the sample age, the rate at which the DSC pan is heated, and the type of sample pan used to prepare the amorphous material. Aged samples exhibit a single exothermic transition at 56 °C, which has been assigned to type I crystallization based on the subsequent melting temperature. The 60–80 °C exotherm was originally thought to result from type II crystallization, but subsequent work is consistent with the assignment of this exotherm to the SCL-to-type III transition, followed by a type III-to-type II transition at approximately 120 °C. In addition to these transitions, a type III-to-type I exotherm has been proposed at 130 °C [14], and it is also well known that thin-film amorphous samples prepared between two glass plates will spontaneously recrystallize to the type III polymorph in the 25–54 °C temperature range [2]. Subsequent heating of type III thin films results in crystallization to the type II polymorph.

Vibrational spectra of all three polymorphs have been measured, and hot stage microscopy has played an important role in elucidating the thermally induced transitions between the four forms (SCL and three polymorphs) of APAP. Using an infrared (IR) microscope coupled to a hot stage, Di Martino et al. [2] measured the infrared (IR) absorbance spectra of temperature-controlled samples that were expected to contain types I, II and III APAP. They observed three distinct vibrational spectra, and assigned the types I and II spectra based on powder X-ray diffraction (PXRD) measurements of the powders. The type III APAP was found to have distinct features in its vibrational structure that confirmed the presence of a third polymorph. Szelagiewicz et al. [10] reported the Raman spectra of types I–III APAP over the 150–1400 cm^{-1} range. They identified features around 1230 cm^{-1} that could be used to distinguish the polymorphs. Subsequently, Wang et al. [15] directly measured thermally induced spectroscopic transformations of IR absorbance spectra from samples of APAP sandwiched between KBr plates. The spectral transformations were assigned to polymorphic transitions by comparing the transition temperatures to DSC thermograms. Al-Zoubi et al. [16] confirmed the assignment of the IR absorbance and Raman spectra of types I and II APAP by reference to the PXRD diffractograms of the samples. Moynihan and O'Hare [17] evaluated the diagnostic value of IR, NMR and Raman spectroscopies for identification of types I and II APAP, and concluded that Raman spectroscopy was not useful for this purpose. However, this is inconsistent with other reports. For example, Raman spectroscopy has recently been shown to be capable of quantitative analysis of the polymorph composition of mixed types I and II APAP powders [18].

Despite these advances in our understanding of thermal transformations of APAP, the interpretation of individual DSC thermograms of APAP remains difficult, because the exothermic transitions that have been assigned to specific polymorphic transformations are very close to one another, and their onset temperatures are influenced by several experimental parameters that are often poorly controlled. The purpose of this paper is to demonstrate the advantage of the simultaneous application of DSC and Raman microscopy for the unambiguous assignment of thermally driven transitions between polymorphs of pharmaceutical materials. Raman detected differential scanning calorimetry (RD-DSC) has been used to monitor the DSC thermogram of SCL APAP and confirms the assignment of two exothermic transitions to specific polymorphic transformations. The influence of the laser excitation source on the measured thermogram has been investigated, and it has been demonstrated that a baseline shift occurs when a polymorphic transformation occurs between crystalline and amorphous forms. Subsequently, the influence of experimental factors on the observed polymorphic transformations has been observed by RD-DSC.

2. Methods and materials

Type I APAP was purchased (Sigma–Aldrich) and used as received. The polymorphic form was confirmed by PXRD and Raman spectroscopy. Type II APAP was prepared by melting several hundred milligrams of type I APAP on a microscope slide at approximately 180 °C, and then rapidly cooling it to room temperature to form the super-cooled liquid (SCL). Upon heating to about 80 °C, the SCL rapidly crystallized. The crystals were found to be the type II polymorph by PXRD and Raman spectroscopy. Heating this material to temperatures exceeding approximately 120 °C resulted in conversion to the type I polymorph. The type III polymorph was prepared by melting a few milligrams of type I APAP on a microscope slide, placing a microscope cover glass on the liquid APAP to form a thin film, and cooling the film to room temperature. The clear film turned white over the course of many hours, and the Raman spectrum of the white material was found to be consistent with published spectra of type III APAP. Low resolution PXRD for polymorph identification was performed with a MD-10 diffractometer (MTI Corporation).

Differential scanning calorimetry (DSC) was performed with a FP 90 controller and a FP84HT hot stage (Mettler-Toledo) with true differential thermal measurement capability. Use of this apparatus allowed simultaneous microscopy and DSC analysis on the same sample. A clear quartz sample crucible was loaded with 10–12 mg of type I APAP, capped with a thin cover glass, and placed on the microscope-accessible sample side of the DSC hot stage. An identical, empty sample pan was used as the thermal reference. The FP 90 controller was used to set the starting temperature, ending temperature, ramp rate and the wait time at each temperature point. The large APAP mass was required for simultaneous microscopy and DSC analysis for two reasons. First, when small quantities of APAP were used, the sample tended to flow to the edge of the sample pan upon melting, and was thereby removed from the microscope field of view. Secondly, because the DSC hot stage is optimized for microscopy rather than sensitivity, higher sample masses are beneficial because they increase the signal-to-noise ratio of the DSC thermograms. DSC thermograms of type I APAP and SCL APAP were reproduced on a Shimadzu DSC-60 calorimeter using small samples (<5 mg) and aluminum sample pans.

Raman microscopy and DSC were performed simultaneously by installing the FP84HT hot stage in a FALCON™ II Wide-field Chemical Imaging System (ChemImage Corp., Pittsburgh, PA). The imaging system was operated in Raman spectral mode, which is capable of collecting full range Raman spectra (350–4000 cm^{-1}) with acquisition times of less than one second. The 532 nm excitation was directed through a 10× objective onto the sample at the beginning of the DSC run. For the RD-DSC experiments described in this study, 1130 W/cm^2 of excitation power was delivered to the sample, and a 10 s acquisition time was used, unless noted otherwise. The ChemImage Xpert™ software (ChemImage Corp., Pittsburgh, PA) was configured for time-based acquisition, which allows the automated collection of multiple spectra with user specified delay between the end of one acquisition and the beginning of the next.

In a typical run, 70–80 Raman spectra were collected, with 10 s acquisition time and 20 s delay, and the DSC was programmed for 5 °C/min ramp rate. Thus spectral acquisition was initiated every 30 s (i.e., every 2.5 °C) and the 10 s acquisition time corresponded to a temperature interval of 0.83 °C. When a DSC ramp rate of 2 °C/min was used, spectral acquisition was initiated every 60 s (i.e., every 2 °C) and the 10 s acquisition time corresponded to a temperature interval of 0.33 °C. The Raman spectra and DSC thermograms were collected independently, and the collection timing was synchronized manually be initiating the Raman acquisition at 10.0 s prior to the beginning of the DSC temperature ramp. Thus the first Raman spectrum was collected at the starting temperature, and the first Raman acquisition was completed at the beginning of the DSC temperature ramp. Each subsequent spectrum was collected at a temperature interval programmed by the user as described above.

Chemometric analysis was performed in Microsoft Excel using high precision math add-ins [19] and routines developed in Visual Basic for Applications. Principal component analysis was implemented using singular value decomposition. Relative sample compositions were determined by multivariate least squares regression of measured spectra to reference spectra using the pseudoinverse formalism, as described below.

3. Results and analysis

Fig. 1 displays the baseline-corrected, normalized Raman spectra of four polymorphic types of APAP (types I–III and the SCL). The spectra have been offset for clarity, and peak frequencies are reported in Table 1. The type I spectrum exhibits characteristic peaks at 1234 and 1325 cm^{-1}, and three well-resolved peaks in the 1500–1700 cm^{-1} range. The type II spectrum shows a pair of weak peaks at 1220 and 1245 cm^{-1}, and a strong peak at 1329 cm^{-1} with peaks in the 1500–1700 cm^{-1} range shifted closer to one another relative to the type I spectrum. The type III spectrum appears similar to the type I spectrum at first glance, but subtle peak shifts are evident in Table 1, and Fig. 1 displays some notable differences in relative peak intensities. Furthermore, it will be shown that the type III spectrum transforms to the type II spectrum at elevated temperature, a transformation that is thermodynamically forbidden for type I APAP. The types I and II spectra are consistent with previous reports. The reported frequencies for types I–III APAP in the 1235 cm^{-1} range are uniformly shifted by 3 cm^{-1} from those reported by Szelagiewicz et al. [10], indicating that the relative peak positions agree with published spectra. Szelagiewicz et al. only reported the Raman spectrum of type III APAP to about 1350 cm^{-1} [10]. The spectrum of the SCL APAP is similar in some respects to the spectra of crystalline APAP, but the peaks appear to be broader, and some peaks are shifted relative to the type I spectrum.

Table 1
Measured peak positions of Raman spectra of the known phases of acetaminophen

Type I (cm^{-1})	Type II (cm^{-1})	Type III (cm^{-1})	SCL (cm^{-1})
654	650	650	645
714	714	693	710
799	799	799	799
837	–	–	833
854	862	862	862
1172	1172	1172	1172
–	1220	–	–
1234	–	–	1233
–	1245	1245	–
1281	1281	1281	1277
1325	1329	1321	1325
1373	1376	1373	1373
1565	1576	1561	1557
1615	1611	1611	1615
–	1623	–	–
1650	1650	1646	–

The types I and II APAP spectra can be visually distinguished by the intensities of the 1234 and 1329 cm^{-1} peaks, and the same peaks can be used to visually distinguish the types II and III spectra. The SCL spectrum can be identified by the weak intensity of the 1325 cm^{-1} peak, and the missing peak at 1650 cm^{-1}.

Fig. 2 displays the RD-DSC thermogram of SCL APAP. The SCL APAP was prepared from type I APAP by heating the calorimeter to 190 °C for 60 s, and then rapidly cooling the crucible to room temperature. The thermogram was collected over the 25–170 °C temperature range at 2 °C/min. Seventy-four Raman spectra were collected simultaneously with 10 s acquisition time and 50 s delay. The straight segment in the thermogram between 30 and 60 °C corresponds to heating of the SCL, which is followed by an exothermic transition with an onset temperature of approximately 63 °C, and a peak at approximately 71 °C. The exothermic transition has concluded by approximately 76 °C, and a large, negative baseline shift is evident on the high temperature side of the exotherm. A small exotherm in the thermogram is barely evident in the 118–127 °C range, and a melting transition is observed with an onset of 155 °C and a peak at 160 °C. The small exotherm at about 120 °C becomes more evident at faster thermal scan rates, as noted by other groups [13,14]. A large, positive baseline shift is also evident on the high temperature side of the melting transition. The 76 °C exotherm, the

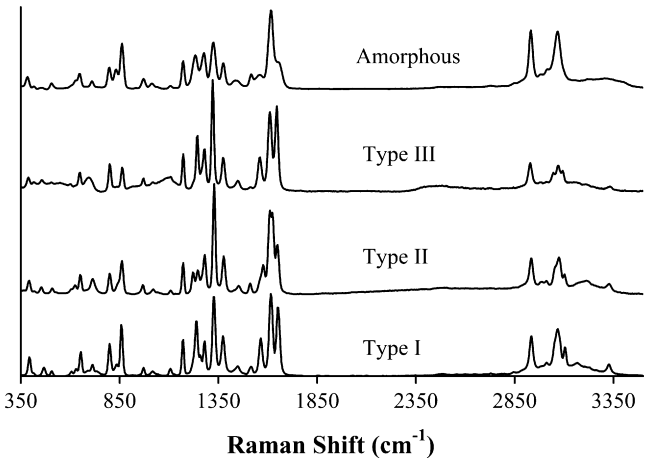

Fig. 1. Full range Raman spectra of the four known phases of acetaminophen. The spectra are offset for clarity.

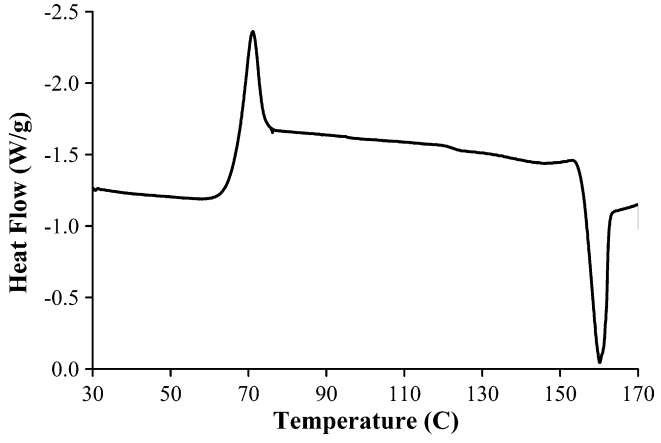

Fig. 2. RD-DSC thermogram of super-cooled liquid acetaminophen in a quartz crucible with glass lid.

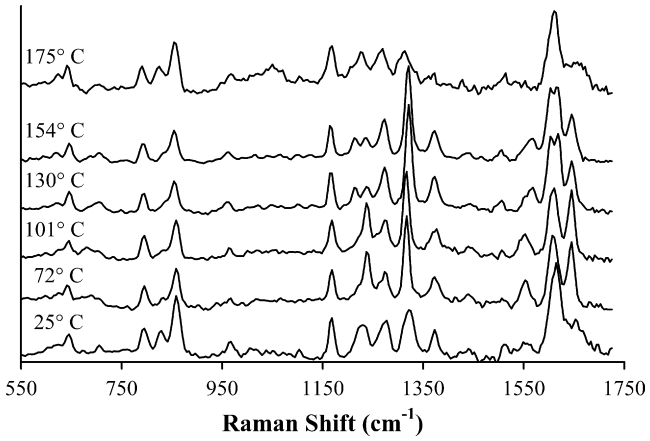

Fig. 3. Selected Raman spectra collected simultaneously with the DSC thermogram shown in Fig. 2. The SCL-to-type III transition occurs between 62 and 72 °C. The type III-to-type II transition occurs between 109 and 120 °C. The spectrum reverts to the amorphous shape above 159 °C.

123 °C exotherm and the 155 °C melting transition are consistent with previous reports [2,13], and have been assigned to the SCL-to-type III transformation, the type III-type II transformation, and the type II melting transition, respectively. The large baseline shift results from the laser irradiation of the DSC sample, and evidence to support this claim will be described below.

Raman spectra from the data set collected simultaneously with the DSC thermogram (Fig. 2) are shown in Fig. 3 at selected temperatures in the fingerprint region. The 25 °C spectrum is identified by the missing 1650 cm^{-1} peak as the spectrum of amorphous SCL APAP. At 72 °C, the spectrum has transformed to a crystalline polymorph. Though it is difficult to distinguish the types I and III polymorphs, the relative intensities of the 1245 and 1321 cm^{-1} bands in combination with the peak position of the peak at approximately 1611 cm^{-1} suggests that the sample has transformed to type III. This polymorph remains until the temperature is raised above 120 °C, at which point the Raman spectrum transforms again. Between 120 and 157 °C, the spectrum is unambiguously assigned to the type II polymorph, based on the structure of the peaks in the in the 1500–1700 cm^{-1} range, the absence of the 1234 cm^{-1} peak, and the intensity of the 1329 cm^{-1} peak. The fact that the type II polymorph is evident at higher temperatures than the putative type III polymorph is consistent with the assignment of the 72 °C transition to the SCL-to-type III transformation. Upon melting, the spectrum returns to that of the amorphous liquid form. These results provide unambiguous assignment of specific transformations observed in Fig. 2, and demonstrate the power of the RD-DSC method.

All 74 spectra collected during the DSC run were subjected to principal component analysis to determine the number of independent factors required to explain the spectra. Fig. 4a displays a scree plot of the first 20 principal components, indicating that the first four principal components explain more than 99% of the spectral variance. Application of the Malinowski *F*-test [20] to the eigenvalues of principal component space also indicates that four principal components explain the systematic spectral variance of the data set. Fig. 4b is a scores plot of the second principal component versus the third principal component, illustrating the evolution of the spectra as temperature increases. The spectral evolution begins at the 25 °C point, and the principal component scores occupy a confined region of scores space associated with the spectrum of the SCL until the temperature reaches 64 °C. The scores then undergo a transition that reflects the APAP phase transformation evident in the DSC thermogram of Fig. 2. At 72 °C, the first phase transition is complete, and the scores evolve within a new confined region of scores space associated with type III APAP. At about 111 °C another transition in scores space occurs corresponding to the type III-to-type II phase transformation. The scores occupy a new confined region of scores space over the 119–159 °C temperature range. Finally, at the melting temperature, the scores evolve toward a region associated with amorphous APAP. Because the spectrum of amorphous liquid APAP differs somewhat from the spectrum of super-cooled liquid APAP, these two phases occupy nearby but distinct regions of scores space, and four principal components are required to explain the data. The evolutionary behavior displayed in Fig. 4b is evident in all pairings of the first four principal components, whereas all scores plots involving the fifth or greater principal components appear random, with no obvious evolutionary behavior. When the distinct phases of a material have different Raman spectra, the principal component scores plot displayed in Fig. 4b can be used to estimate the number of distinct phases in the DSC as well as the initial and final phase transformation temperatures, even when the Raman spectra of the pure phase components are not known. Even weakly exothermic transformations such as the type III-to-type II APAP transformation can be clearly identified in the principal component scores plot when the Raman spectra of the two phases are different from one another.

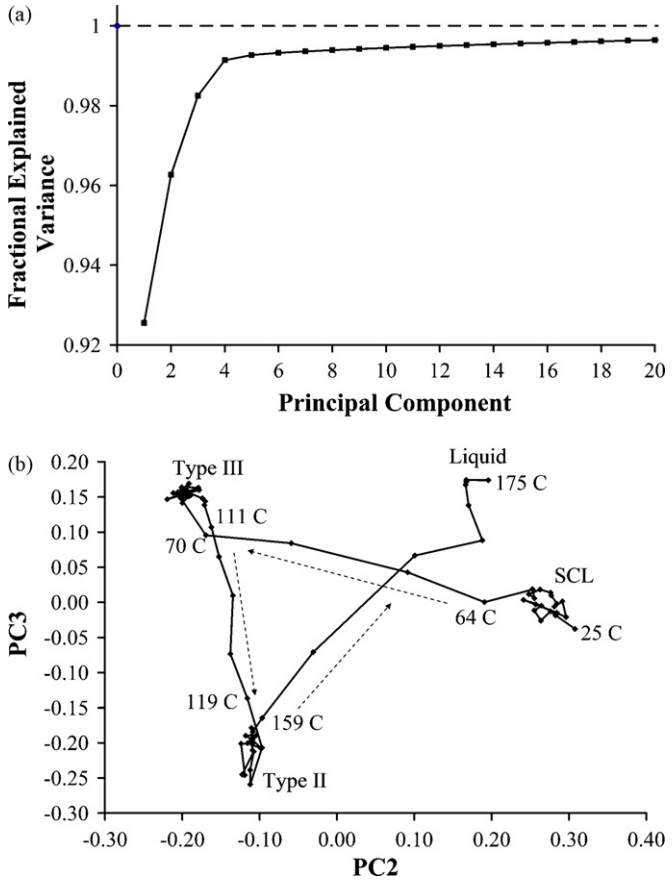

Fig. 4. (a) Scree plot showing the cumulative variance explained by the first 20 principal components of the Raman spectra measured during the RD-DSC shown in Fig. 2. The plot demonstrates that four principal components can explain the systematic spectral variance in the data. (b) Scores plot showing the evolution of the principal component scores of the Raman spectra measured during the RD-DSC shown in Fig. 2. Spectral collection begins at 25 °C, and the temporal evolution of the scores follows in the direction of the arrows. Scores clusters are evidence of distinct phases, and the evolution between clusters occurs over temperature ranges characteristic of the phase transitions.

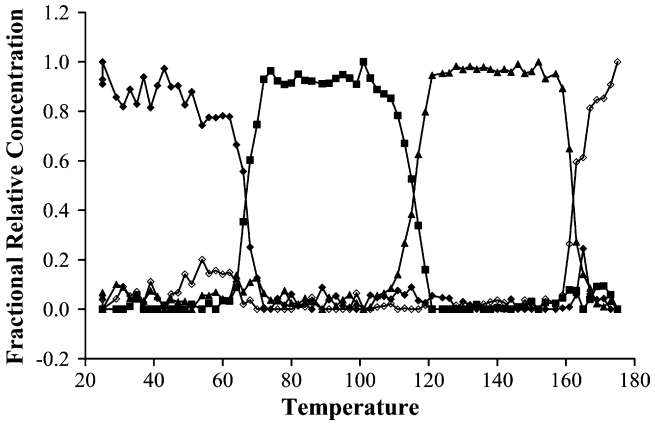

Fig. 5. Fractional contributions of SCL APAP (♦), type III APAP (■), type II APAP (▲) and liquid APAP (◊) to the sample composition as a function of DSC temperature.

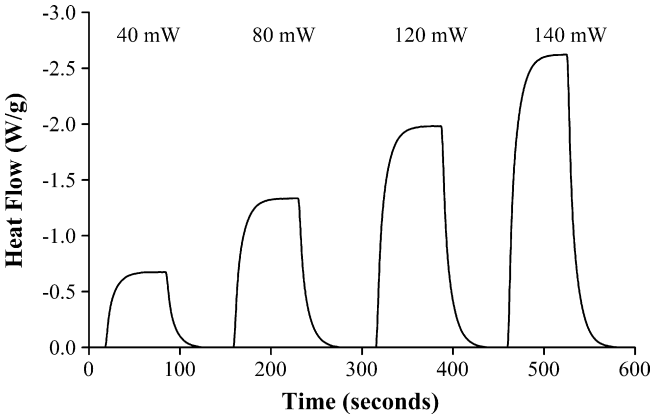

Fig. 6. Laser induced time-dependent heat flow curves. When the laser is turned on, it irradiates the sample side sensors, and heat flows from the sample side of the DSC to the reference side, resulting in an apparent exothermic event. The heat flow reaches a steady state within 60 s after laser irradiation is initiated. The power values are the laser powers delivered to the DSC for each of the 4 events.

Additional information can be gleaned from multivariate analysis of the spectral data if the pure component Raman spectra of the phases are known, as in the case of APAP. Multivariate least squares regression of the spectra measured during RD-DSC was performed against a set of four phase-specific APAP reference spectra including SCL, type III, type II and liquid APAP, to give a set of four coefficients at each temperature that reflect the contribution of each of the four phases to the Raman spectrum measured at that temperature. The resulting fractional contributions of the four phases are displayed as a function of temperature in Fig. 5. The estimated root mean squared deviation of the data was 0.06, and for coefficients near zero, physically forbidden negative values of up to −0.1 were observed. Negative coefficients were set equal to zero, and the resulting coefficients were normalized so that the sum of all coefficients at each temperature equaled one. For temperatures between 25 and 60 °C and above 159 °C, both the SCL and the liquid APAP spectra appear to contribute to the sample spectrum. This reflects the fact that the linear regression cannot always distinguish the spectral contribution of the amorphous super-cooled liquid from the contribution of the molten liquid, because their spectra are very similar to one another. With this exception, the only temperature regions that exhibit more than one phase are the phase transition temperatures. The temperature dependence of the relative compositions can also be used to characterize phase transformation temperatures. For example, the crossover points between SCL and type III (67 °C), types III and II (116 °C) and type II and liquid APAP (162 °C) provide estimates of the phase transformation temperatures.

Fig. 6 displays a series of time-dependent heat flow curves measured while irradiating an empty crucible in the DSC hot stage with the Raman excitation source. When the laser is turned on, a negative heat flow is observed, and the heat flow reaches a steady state in approximately 50 s. When the laser is turned off, the heat flow returns to zero. The steady state heat flow is linearly dependent on the laser power, and reflects the fact that when the laser passes through the hot stage crucible, a small amount of scattered light falls on the sample-side thermal sensors. Heat must flow from the irradiated sample side to the dark reference side in order to achieve thermal balance. The linear dependence of laser-induced heat flow from an empty crucible demonstrates that the magnitude of the heat flow will depend on the amount of light scattered by the sample, which in turn depends on the polymorphic phase of the sample. To test this hypothesis, the following experiments were performed on a fresh SCL APAP sample prepared in a quartz crucible. Fig. 7a displays the time-dependent laser-induced heat flow curve at room temperature, in which the laser is directed through the translucent SCL APAP sample for approximately 60 s. During this time the heat flow reached a steady state of −30 W/g. Following this measurement, the laser irradiation was turned off, and the DSC thermogram of the sample was measured at a ramp rate of 10 °C/min. Fig. 7b displays the 70 °C exothermic transition measured with the FT84HT DSC hot stage in the absence of Raman excitation. It shows an onset temperature of about 55 °C, a peak of about 68 °C, and the transition is complete by about 75 °C. A small baseline shift is evident, and is related to the differential thermal conductivity between the amorphous and crystalline forms. After the phase transition, the laser-induced time dependent heat flow was measured again, and the result is shown in Fig. 7c. The magnitude of the laser induced heat flow increased to −70 W/g following transformation of the sample from the translucent SCL to the light scattering crystalline polymorph. These observations explain the large negative baseline shift that occurs in Fig. 2 upon crystallization of the SCL at about 70 °C. In Fig. 2, the baseline shifts in the positive direction on the high temperature side of the melting transition at 160 °C, because the sample becomes translucent again after melting, and reduces the intensity of scattered light irradiating the thermal sen-

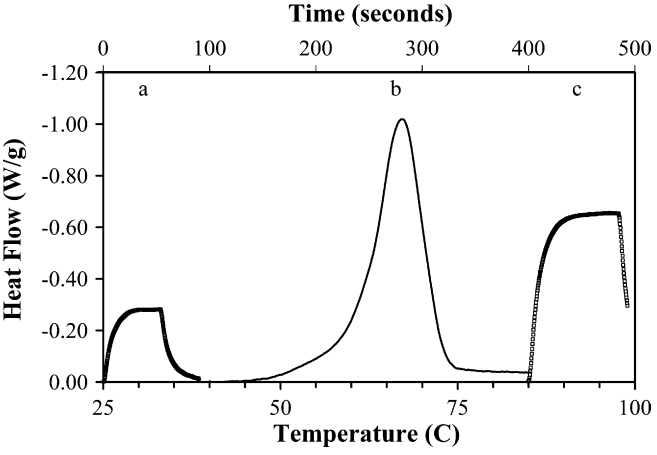

Fig. 7. Time-dependent heat flow curves superimposed on the DSC thermogram of SCL APAP in the SCL-to-type III region. (a) Heat flow curve for excitation of the transparent SCL. (b) DSC thermogram of the SCL-to-type III transition without laser excitation. (c) Heat flow curve for excitation of the type III polymorph. The steady state heat flow increases by a factor of 2.3 when the APAP transforms from the SCL form to the type III crystalline form. Without laser excitation, the DSC exotherm exhibits a small baseline shift.

sors. These observations are consistent with the hypothesis that baseline offsets observed in RD-DSC result from the polymorphic phase dependence of the amount of scattered light that irradiates the sample-side thermal sensors.

4. Discussion

Several APAP samples have been examined with RD-DSC in this study under a variety of conditions, which allow us to confirm the results of previous studies with the polymorphic specificity of Raman spectroscopy. For example, an aged SCL sample (55 days at room temperature) was found to have spontaneously transformed to type II APAP at room temperature. When RD-DSC was performed on this sample at a ramp rate of 5 °C/min from 30 to 200 °C, the Raman spectra showed that the sample transformed to type I APAP at 85 °C, but an exothermic transition was not evident in the DSC thermogram. As a second example, it was also found that if the RD-DSC of APAP was performed on samples in quartz crucibles without lids, type III APAP was not observed, and the SCL-to-type II transition occurred at temperatures between 45 and 55 °C, accompanied by a large exotherm in the DSC, but without the appearance of the type III intermediate. Furthermore, if the SCL was prepared in a crucible without a lid, and then covered with a lid after the SCL was returned to room temperature, type III APAP was still not observed. But if the same sample was thermally cycled to prepare the amorphous SCL sample with the lid in place, the thermogram shown in Fig. 2 reappeared. These observations suggest that thin films of APAP form between the lid and the crucible during the DSC SCL preparation cycle, and that such films foster the formation of type III APAP from the SCL. It is likely that similar films can form at the seam of standard aluminum crimp pans that are commonly used with other DSC instruments. An additional type II-to-type I transformation was occasionally found to occur at temperatures ranging from 70 to 135 °C. This appeared to be correlated with the low temperature SCL-to-type II transformation, although the conditions that favored the low temperature type II-to-type I transformation have not yet been unambiguously identified. The work presented here confirms the fact that seemingly unimportant experimental variables can influence the transformations that are observed during DSC of SCL APAP, and highlights the need for methodology that both reports thermal events associated with phase transformations and allows the identification of the phases involved.

Using standard DSC, the thermal output of a phase transformation is evident from the DSC thermogram, but additional methods must be employed to identify the phases. RD-DSC combines these two tasks, and allows the analyst to observe phase transformations whose thermal outputs are below the thermal detection limit of the DSC instrument. It also allows the analyst to assign thermally driven phase transformations to specific phases of the material under study in real time during the measurement of the DSC thermogram. The RD-DSC method has two significant limitations. First, it is only applicable to samples whose phases display distinct Raman spectra. Secondly, sample fluorescence can hinder the application of RD-DSC to compounds that are fluorescent or contain fluorescent impurities. The influence of fluorescence was evident in the course of this study, because repeated thermal cycling of APAP resulted in pink-colored impurities that contributed significantly to the fluorescence background in the Raman spectra. After three thermal cycles the APAP sample had to be discarded. In addition to these limitations, the data shown in Figs. 6 and 7 indicate that care must be taken in the interpretation of baseline offsets when RD-DSC is employed, and it is also likely that the baseline offset will skew the peak positions and apparent onsets of thermal events in the DSC trace. Though these effects can be partially mitigated by principal component analysis and multivariate regression of the Raman spectra, RD-DSC is not likely to produce highly accurate calorimetric quantities. Nevertheless RD-DSC offers significant benefit as a method to establish the number of distinct phases contributing to a DSC thermogram as well as qualitative assignment of those phases to specific polymorphic forms.

References

[1] G. Nichols, C.S. Frampton, J. Pharm. Sci. 87 (1998) 684–693.
[2] P. Di Martino, P. Conflant, M. Drache, J.P. Huvenne, A.-M. Guyot-Hermann, J. Therm. Anal. Calorim. 48 (1997) 447–458.
[3] P. Di Martino, A.-M. Guyot-Hermann, P. Conflant, M. Drache, J.-C. Guyot, Int. J. Pharm. 128 (1996) 1–8.
[4] M.L. Peterson, S.L. Morissette, C. McNulty, A. Goldsweig, P. Shaw, M. LeQuesne, J. Monagle, N. Encina, J. Marchionna, A. Johnson, J. Gonzalez-Zugasti, A.V. Lemmo, S.J. Ellis, M.J. Cima, O. Almarsson, J. Am. Chem. Soc. 124 (2002) 10958–10959.
[5] T. Beyer, G.M. Day, S.L. Price, J. Am. Chem. Soc. 123 (2001) 5086–5094.
[6] J.-M. Fachaux, A.-M. Guyot-Hermann, J.-C. Guyot, P. Conflant, M. Drache, S. Veesler, R. Boistelle, Powder Technol. 82 (1995) 123–128.
[7] J.-M. Fachaux, A.-M. Guyot-Hermann, J.-C. Guyot, P. Conflant, M. Drache, S. Veesler, R. Boistelle, Powder Technol. 82 (1995) 129–133.
[8] E. Joiris, P. Di Martino, C. Berneron, A.-M. Guyot-Hermann, J.C. Guyot, Pharm. Res. 15 (1998) 1122–1130.
[9] M. Lang, A.L. Grzesiak, A.J. Matzger, J. Am. Chem. Soc. 124 (2002) 14834–14835.
[10] M. Szelagiewicz, C. Marcolli, S. Cianferani, A.P. Hard, A. Vit, A. Burkhard, M.V. Raumer, U.C. Hofmeier, A. Zilian, E. Francotte, R. Schenker, J. Therm. Anal. Calorim. 57 (1999).
[11] P. Di Martino, G.F. Palmieri, S. Martelli, Chem. Pharm. Bull. 48 (2000) 1105–1108.
[12] W.J. Sichina, Am. Lab. (January 2001).
[13] S. Qi, P. Avalle, R. Saklatvala, D.Q.M. Craig, Eur. J. Pharm. Biopharm. 69 (2008) 364–371.
[14] A. Rossi, A. Savioli, M. Bini, D. Capsoni, V. Massarotti, R. Bettini, A. Gazzaniga, M.E. Sangalli, F. Giordano, Thermochim. Acta 406 (2003) 55–67.
[15] S.L. Wang, S.Y. Lin, Y.S. Wei, Chem. Pharm. Bull. 50 (2002) 153–156.
[16] N. Al-Zoubi, J.E. Koundourellis, S. Malamataris, J. Pharm. Biomed. Anal. 29 (2002) 459–467.
[17] H.A. Moynihan, I.P. O'Hare, Int. J. Pharm. 247 (2002) 179–185.
[18] K. Kachrimanis, D.E. Braun, U.J. Griesser, J. Pharm. Biomed. Anal. 43 (2007) 407–412.
[19] L. Volpi, XNumbers-Multiprecision Floating Point Computation and Numerical Methods for EXCEL [4.5], Foxes Team, 2005.
[20] E.R. Malinowski, Factor Analysis in Chemistry, John Wiley and Sons, New York, 2002, pp. 104–107.